Size selective spectroscopy of Se microclusters

Kooser, K.; Ha, D. T.; Itala, E.; Laksman, Joakim; Urpelainen, Samuli; Kukk, E.

Published in:
Journal of Chemical Physics

DOI:
10.1063/1.4737633

2012

Size selective spectroscopy of Se microclusters

K. Kooser, D. T. Ha, E. Itälä, J. Laksman, S. Urpelainen et al.

Citation: J. Chem. Phys. **137**, 044304 (2012); doi: 10.1063/1.4737633
View online: http://dx.doi.org/10.1063/1.4737633
View Table of Contents: http://jcp.aip.org/resource/1/JCPSA6/v137/i4
Published by the American Institute of Physics.

Size selective spectroscopy of Se microclusters

K. Kooser,[1,a)] D. T. Ha,[1,2] E. Itälä,[1,2] J. Laksman,[3] S. Urpelainen,[4,5] and E. Kukk[1,6]
[1]*Department of Physics, University of Turku, FIN-20014 Turku, Finland*
[2]*Graduate School of Materials Research, Turku, Finland*
[3]*Department of Synchrotron Radiation Research, Lund University, Sölvegatan 14, SE-22362 Lund, Sweden*
[4]*MAX-lab, Lund University, P.O. Box 118, SE-22100 Lund, Sweden*
[5]*Department of Physics, University of Oulu, Box 3000, FIN-90014 Oulu, Finland*
[6]*Turku University Centre for Materials and Surfaces (MatSurf), Turku, Finland*

(Received 10 April 2012; accepted 3 July 2012; published online 25 July 2012)

The electronic structure and photofragmentation in outer and inner valence regions of Se_n ($n \leq 8$) clusters produced by direct vacuum evaporation have been studied with size-selective photoelectron-photoion coincidence technique by using vacuum-ultraviolet synchrotron radiation. The experimental ionization potentials of these clusters were extracted from the partial ion yield measurements. The calculations for the possible geometrical structures of the Se_n microclusters have been executed. The ionization energies of the clusters have been calculated and compared with the experimental results. In addition, theoretical fragment ion appearance energies were estimated. The dissociation energies of Se_n clusters were derived from the recurrent relation between the gas phase enthalpies of the formation of corresponding cationic clusters and experimental ionization energies. © *2012 American Institute of Physics*. [http://dx.doi.org/10.1063/1.4737633]

I. INTRODUCTION

The evolution of the electronic states and properties in microclusters (containing less than a few hundred atoms) has drawn great attention due to their fundamental interest in basic research as well as the possibility of constructing nanostructured materials and devices using clusters as building blocks. The basic aim is to gather information about the unique chemical and physical properties of the clusters, which compared to the single atoms and solids have intermediate nature. One of the central questions in cluster physics is, how the number of atoms in a specific cluster determines its electronic properties. In spite of the possibility to use different cluster formation methods (for example, pulsed supersonic expansion, inert gas condensation, or laser vaporization), the study of microclusters is usually limited because of the fact that cluster beams cannot be generated in a single adjustable cluster size.

The chemistry of the chalcogen (such as S, Se, Te) clusters is an area of growing relevance because of their usefulness in the miscellaneous applications. For example, it has been shown that nanostructured selenium is a promising mercury sorbent that may be applied in cleanup, disposal, recycling and packaging applications,[1] and that Se nanoclusters have the potential as a chemopreventive Ti orthopedic material coating.[2] Also, there has been reported that the microbiologically formed nanorods composed of elemental tellurium forms unusual nanocomposites when combined with an organic chemical host.[3] These bio-nanocomposites are likely to form a new class of nanomaterials for the future nanoelectronic and nanophotonic applications. The properties of these nanomaterials are mainly caused by the ability of chalcogenes to form polyatomic complex chains and rings of a variety of sizes and shapes. While moving in the periodic table from sulfur toward tellurium the gradual changes in the structural preferences of the different elements appear, which influence the physical properties of their microclusters.[4,5]

Until now the equilibrium geometries, energetics, and vibrational frequencies of the neutral and cationic Se_n ($2 \leq n \leq 8$) clusters have been investigated by exploiting different theoretical approaches.[6–9] The experimental investigation of the valence electronic structure of the Se microclusters produced by the adiabatic expansion method and using the N_2-flashlamp at energy 10.0 eV (Ref. 10) as well as electron impact ionization on Se clusters in the size range from 2 to 36 has been performed.[11] The photothermodissociation of small Se cluster ions produced by a gas aggregation source, ionized, and heated up by a pulsed excimer laser have been studied.[12] Also photofragmentation study of selenium cluster cations produced by combination of laser vaporization and supersonic expansion[13] can be found.

In order to explore the electronic properties of the Se_n ($n \leq 8$) microclusters as a function of their size, in this study a mass-selective photoelectron-photoion coincidence (PEPICO) setup has been used.[14] The aim of this work is to explore, accurately, the evolution of the electronic structure of Se clusters produced by the direct vacuum evaporation technique as a function of the cluster size. We present the results of the experimental study of the ionization and fragmentation of Se_n clusters after valence photoionization, using the partial ion yield (PIY) and PEPICO techniques. For the interpretation of these results, *ab initio* electronic structure calculations of the binding and appearance energies of selenium clusters and their fragments are carried out and compared with the experimental outcomes.

The application of PIY technique for the exploration of neutral clusters over the vacuum ultraviolet (VUV) photon

a)Electronic mail: kunkoo@utu.fi.

energy range yields valuable information for the accurate determination of adiabatic ionization energies and ion appearance energies.[15] The data recorded by using PEPICO technique and extracted to the form of coincidence ion yields (CIYs) represent the intensities of ionized clusters as a function of the coincident electron's binding energy.[16] The curves of CIYs enable to unravel in detail the valence electronic structure of the ionized clusters. The CIYs may also contain the complex signal of the fragmented cluster ions originated from bigger clusters. The integration of the theoretical CIY spectrum, assuming constant photoionization cross section and absence of dissociation channels, generates a corresponding PIY curve. Here the advantages of PIY technique such as a shorter recording time and an excellent energy resolution for determination of ion appearance energies have been used. PEPICO method was employed for the examination of the electronic structure of ionized clusters and for studying of possible fragmentation channels.

II. EXPERIMENT

The measurements were performed at the FinEst branchline at the normal incidence monochromator beamline I3 of MAX-III synchrotron storage ring (Lund, Sweden).[17,18] In this work the experimental PEPICO setup[19] consisting of a modified Scienta SES-100 electron analyser[20] and a homemade Wiley-McLaren type ion time-of-flight (TOF) detector was used.

Briefly, the original CCD-camera-based detection system of the electron spectrometer was replaced by a resistive anode detector (Quantar) in order to achieve fast single electron position-sensitive response signal in a nanosecond scale. The ion TOF spectrometer is equipped with a 77 mm active area Hamamatsu microchannel plate detector followed by 10 concentric anode rings to enable the registration of the longitudinal and radial time-of-flight components of the ions relative to the symmetry axis of the ion spectrometer tube. The ion detection electronics is based on a 1 GHz waveform digitizer card (Signatec PDA 1000). The PEPICO measurements were performed in a pulsed field mode, where the detection of the electron by the electron analyzer triggers the clock for the TOF of the ions (true coincidences), within a certain time window. However, the ion TOF spectrometer detects also the fragments (false coincidences or noncoincidences) which are not created from the molecule that initially ejected the detected photoelectron. For the extraction of the coincidence and noncoincidence events, the experimental setup contains also an additional pulse generator which provides artificial extraction pulses at a constant frequency. During the PEPICO experiment both – the electron and artificially triggered events, and the coincidence and noncoincidence data maps, respectively, were recorded. Finally, a custom made IGOR PRO software based data analysis macros were used to subtract the false coincidence background from the initial coincidence map and retrieve the real coincidence data pattern.

The PEPICO system was operated in the pulsed extraction field mode and in the present experiment the extraction pulse voltage was ± 300 V across the sample region, with the drift tube held at -1680 V. The entrance slit of the electron spectrometer was 1.6 mm and the pass energy was 50 eV, which gives a resolution of 0.4 eV. The base pressure in the end-station chamber was less than 5×10^{-7} mbar. During the experiment the chamber pressure was maintained below 2×10^{-6} mbar.

In order to retrieve the PIYs the time-of-flight mass spectra were collected at the photon energies in the range of 7.0–10.0 eV with an energy step of 0.05 eV. In each time-of-flight mass spectrum 100 000 triggers (or events) was recorded. The PIYs were obtained by selecting the time-of-flight window of an ion peak from the dataset of time-of-flight mass spectra and by integrating the ion counts at each photon energy. The photon flux used for spectra normalization was measured by a photodiode. A LiF crystal was used to block the higher harmonics of the undulator radiation. The absorption spectrum of Ar gas was used for the photon energy calibration of the PIY spectra.

The Se sample was purchased from Sigma-Aldrich with the purity greater than 99.99% and evaporated into the interaction area of the spectrometers from a boron nitride crucible of effusion cell with integrated cooling shroud (MBE Komponenten NTEZ-40) at the temperature around 240 °C.

III. RESULTS

A. Partial ion yields of Se microclusters

A typical TOF Se_n mass spectrum obtained at the ionization energy of 10 eV is given in Figure 1. All peaks of the TOF mass spectra gathered in this experiment are calibrated with the TOF maxima of rest gases such as H_2O, N_2, and O_2. It is possible to identify 7 different Se_n^+ species, where $2 \leq n \leq 8$. Every broad Se cluster peak of a given size consists of the sharper peaks caused by the isotopic distribution of selenium (0.84% of ^{74}Se, 9.36% of ^{76}Se, 7.63% of ^{77}Se, 23.78% of ^{78}Se, 49.61% of ^{80}Se, and 8.73% of ^{82}Se). The peak analysis of Se cluster ions in the measured TOF spectra confirmed this expected isotopic distribution. The measured relative abundances of the clusters at $h\nu = 10$ eV are: $Se_2 : Se_3 : Se_4 : Se_5 : Se_6 : Se_7 : Se_8 = 0.132 : 0.009 : 0.015 : 0.334 : 0.407 : 0.086 : 0.018$ The comparison of the abundances of our direct vacuum evaporation products with the outcome of Se clusters produced by the

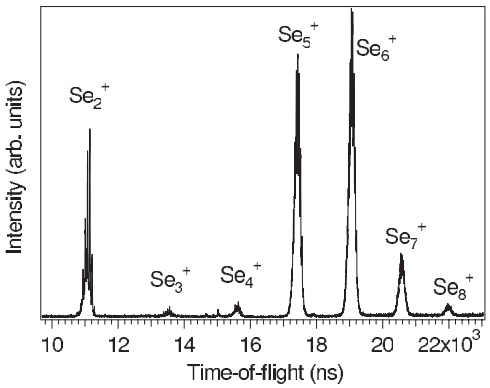

FIG. 1. The TOF spectrum of Se_n clusters ($n = 2 - 8$) measured at the ionizing photon energy of 10 eV; the temperature of evaporation oven at around 240 °C.

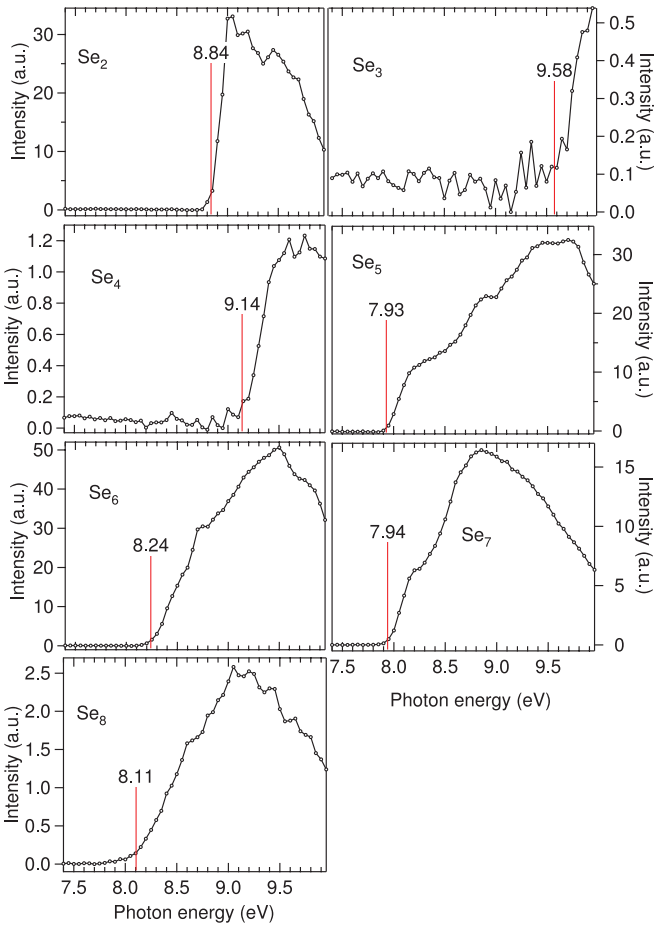

FIG. 2. The PIY spectra of Se_n clusters ($n = 2 - 8$) measured at the valence region threshold. The vertical red lines represent the positions of ionization energies together with numerical values.

supersonic molecular beam technique[10] at the same excitation energy shows some clear differences in the composition of the selenium vapor. The intensity of the ion TOF peaks corresponding to the Se_2 clusters is much higher in the case of direct vacuum evaporation and has almost the same magnitude as for the clusters Se_5, Se_6. The abundancies of the Se_3, Se_4 clusters have not been detected in the supersonic molecular beam evaporation process (at $h\nu = 10$ eV). In the direct vacuum evaporation process the intensities of Se_5, Se_6 cluster peaks are the strongest and the intensity of the TOF peak corresponding to the Se_7 clusters is much weaker. The Se_5 clusters are most abundant also if the supersonic molecular beam technique is used, but the intensity of Se_6 cluster peak was suppressed to the same level as for Se_7. The estimation of the signal ratio Se_2^+/Se_8^+ for direct evaporation experiment and for supersonic molecular beam technique gives approximate values 7 and 2, respectively.

The partial ion yields of Se_n clusters measured in the photon energy range from 7.5 eV to 10 are shown in Figure 2. Due to the high efficiency of the TOF mass spectrometer, it was possible to extract PIY curves for the main cluster species with a very good signal-to-noise ratio and to detect the less abundant clusters. In order to provide a complete set of information from the photoionization efficiency curves of Se clusters produced by direct vacuum evaporation, the background signal of lighter mass-fragments is subtracted from each PIY of the Se_n cluster ($n = 1 - 8$).

In the photon energy range up to 10 eV a signal from all Se clusters Se_{1-8} was detected. A strong signal from the cluster ions Se_2, Se_5, Se_6, Se_7 has been detected, whereas the PIYs of Se_3, Se_4 and Se_8 clusters have much weaker signal on an absolute scale and the weakest Se_1 signal (not given in Figure 2) is detectable only above 9.75 eV. The onsets and shapes of PIYs show strong dependence on the size and parity of cluster. Using a linear extrapolation method, the ion appearance energies (AE) for all Se_{1-8} clusters have been determined. The comparison of the obtained AE values with the earlier studies of Se clusters is given in Table I. Note that the AEs of the ions are equivalent to adiabatic cluster ionization energies only if the ions are not produced by fragmentation. In Refs. 10 and 11, the term ionization potential, what is a synonym to the adiabatic ionization energy, has been used.

The given values of AEs from different experiments vary slightly depending on the growth method of the clusters. In other words, it cannot be excluded that the size distribution of the small Se clusters in the vapor is strongly affected by the initial evaporation and nucleation conditions. Furthermore, the values of the ionization energies as indicators of the structural (or geometrical) properties of the clusters given in Table I may indicate the presence of different isomeric distribution due to the experimental thermodynamic conditions. The geometry and conditions for creation and appearance of Se trimers and tetramers are probably the most affected by these circumstances in various experiments.

TABLE I. Appearance energies of Se_n ($n = 1$–8) clusters or fragments in electronvolts from different experiments.

n	This work (VUV photon impact) Direct evaporation method	From Ref. 10 (VUV photon impact) Supersonic expansion method	From Ref. 11 (electron impact) Supersonic expansion method
1	9.75 ± 0.05	...	...
2	8.84 ± 0.05	8.7 ± 0.2	8.3 ± 0.3
3	9.58 ± 0.05	...	9.2 ± 0.3
4	9.14 ± 0.05	...	9.1 ± 0.3
5	7.93 ± 0.05	7.6 ± 0.2	8.3 ± 0.3
6	8.24 ± 0.05	7.9 ± 0.2	8.4 ± 0.3
7	7.94 ± 0.05	7.6 ± 0.2	8.2 ± 0.3
8	8.11 ± 0.05	7.8 ± 0.2	8.4 ± 0.3

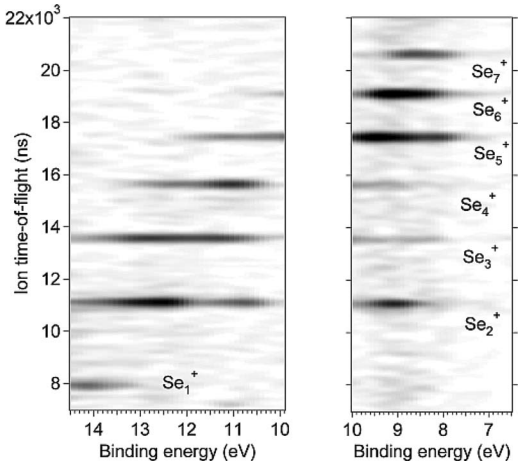

FIG. 3. PEPICO maps of selenium clusters recorded in coincidence with Se valence photoionization

B. Photoelectron-photoion coincidence pattern of valence region of the Se microclusters

In Figure 3 the PEPICO maps of Se_n cluster ions in coincidence with Se valence photoelectrons are represented. The values of the vertical axis of the plot correspond to the coincident ionized cluster time-of-flight and the horizontal scale represents the characteristic energy of coincidence electrons. Ion counts are represented in the grayscale. Here a binding energy scale is used, corresponding one-to-one to the experimentally measured kinetic energy of electrons. The patterns have been recorded separately in two adjacent kinetic energy windows (E_{center} = 10.2 eV and 13.5 eV (or ΔE_{center} = 3.3 eV)) of the electron spectrometer at the pass energy of 50 eV.

The ionizing photon energy equal to 22 eV, below the double ionization threshold of Se (Ref. 21) was chosen.

The coincidence signals from all eight selenium clusters (from Se_1 up to Se_8) were detected. Here the pattern of Se_8^+ is left out from Figure 3 due to a very low intensity and blurred trace, though an evidence for the presence of Se_8 clusters is given in Sec. III A by results of photoionization efficiency curves (see the lowest left panel in Figure 2). The examination of both PEPICO maps indicates a strong variance of coincidence pattern depending on the size of the cluster. The map of the upper valence region (the right one in Figure 3) contains intense signals from the clusters Se_2^+, Se_5^+, Se_6^+, and Se_7^+, the intensities from Se_3^+ and Se_4^+ are much weaker in this binding energy range. As the binding energy of coincident electrons increases (the left map in Figure 3), the signal from the ions of trimers and tetramers increases remarkably and at around 12.5 eV also the first detectable signal of Se_1^+ ion appears. The intensities of Se_7^+, Se_6^+ ions drop to zero above 10.5 eV in the binding energy scale and only a weak tail of signal from Se_5^+ ions remains. Only the coincidence signal from Se_2^+ ions is present in the whole detected binding energy range. The appearance of the coincidence patterns of Se_1^+, Se_2^+, Se_3^+, and Se_4^+ cations in a higher binding energy range suggests the fragmentation of larger clusters such as Se_8, Se_7, Se_6, and Se_5, as discussed in Sec. IV.

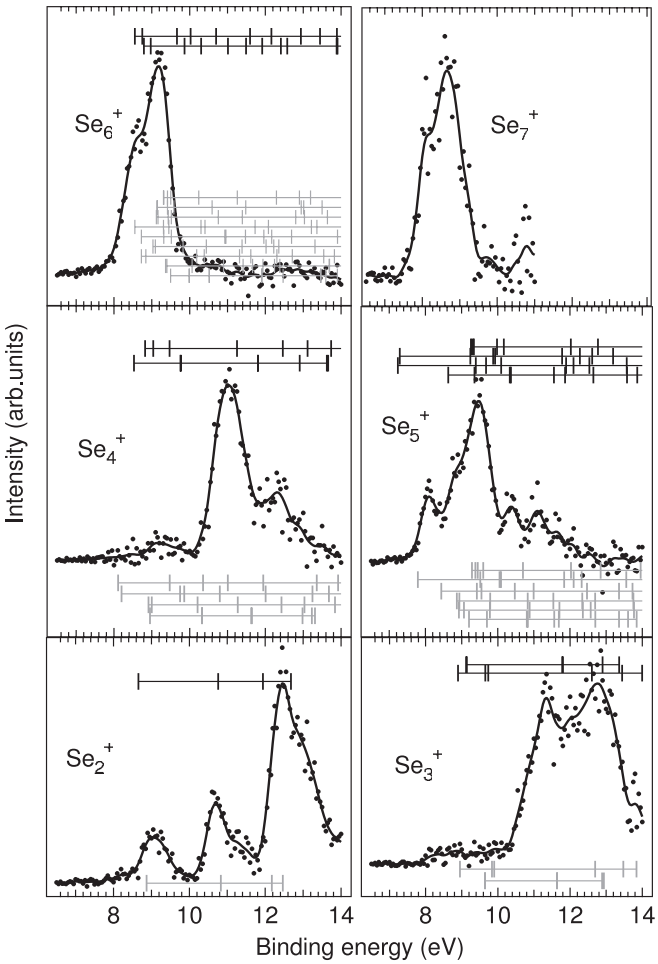

FIG. 4. The CIY spectra of Se_n clusters (n = 2–7) measured at photon energy 22 eV. The experimental data (black dots) are represented together with smoothed guide (solid) lines. The long horizontal bars present the total energy levels of isomers and every tiny vertical bar on a long bar stands for a molecular orbital (MO) energy level of corresponding cluster isomer. The calculation results of restricted open-shell Hartree-Fock theory (grey bars) are depicted below the corresponding CIY curve and the results of the unrestricted Hartree-Fock with second-order Møller-Plesset method (black bars) are given above the CIY spectrum. The maximum of counts (or coincidence events) 890 for Se_2, 430 for Se_3, 480 for Se_4, 520 for Se_5, 430 for Se_6 and 110 for Se_7 have been detected.

The data of the PEPICO maps in Figure 3 were also extracted to the form of CIYs, representing the cluster intensities as a function of the coincident electron's binding energy. In Figure 4 the CIYs of the Se_n^+ (n = 2–7) clusters are shown, corresponding to the photoionization at 22 eV.

The spectrum of ionized Se_2 dimer (bottom left panel of Figure 4) has three strong peaks at binding energies 9.0 eV, 10.7 eV, and 12.5 eV. The last two maxima have shoulders at energies 11.3 eV and 13.1 eV. The valence molecular orbital configuration of Se_2 can be represented, in the ground state, by

$$\ldots (\sigma_g 4s)^2 (\sigma_u 4s)^2 (\sigma_g 4p)^2 (\pi_u 4p)^4 (\pi_g 4p)^2. \quad (1)$$

The first band at 9.0 eV may be identified as ionization from the outermost $(\pi_g 4p)^2$ orbital, leaving the ion in the $X^2\Pi_g$ state, which has spin-orbit split components $^2\Pi_{g,1/2}$

and $^2\Pi_{g,3/2}$ identified by Streets *et al.*[22] at the binding energies 8.89 eV and 9.13 eV (they are not resolvable in this study due to the lower resolution of the electron spectrometer). Similarly, according to the same Ref. 22, the next structure between 10 eV and 12 eV corresponds to the ionization of an electron from the second highest orbital ($\pi_u 4p$) and the resolvable peaks at 10.7 eV and 11.3 eV may be interpreted as the $a^4\Pi_u$ and $A^2\Pi_u$ states, respectively. Additionally, the results of photoelectron spectroscopy of Se_2 dimer by Streets *et al.*[22] show sharp peaks at 12.27 eV, 13.31 eV, and 14.00 eV, assigned to the $^4\Sigma_g^-$, $^2\Sigma_g^-$, and $^2\Pi_u^{(3)}$ states. The CIY of Se_2 cations of the present study contains only one clear peak at 12.5 eV with a shoulder at 13.1 eV. However, this huge peak is remarkably stronger than the structures at lower binding energies. Additionally, there are detected strong TOF peaks of Se_5^+, Se_6^+, and Se_7^+ clusters (see Figure 1). These differences in the CIY spectrum are indicators for a strong contribution from Se_2^+ fragments, created by the dissociation of the larger Se clusters, in a binding energy range from 12 to 14 eV.

The CIY of ionized Se_3 trimer has a very low intensity below 10.2 eV and a broad band extending up to 14 eV in binding energy scale. The band contains two maxima at about 11.4 eV and 12.8 eV. The intensity of Se_4 tetramer ions is also low below 10.2 eV and has a weak visible maximum at around 9.1 eV. The CIY of Se_4^+ shows a strong peak at 11.1 eV and more than two times weaker maximum at 12.3 eV.

Let us consider the CIYs of Se_5^+, Se_6^+, and Se_7^+ jointly. The CIY curve of Se_5^+ has the first peak at 8.1 eV and the second at 9.5 eV with a shoulder located at 8.8 eV. The intensity of the yield is remarkably lower above 10 eV, but has still two peaks at 10.4 eV and 11.1 eV. The comparison of the CIY of the Se_5^+ with the result of Becker *et al.*[10] shows energetically small but visible differences. The first peak of the coincidence photoelectron spectrum of the Se_5 cluster in Ref. 10 is located 0.2–0.3 eV towards lower binding energy compared to the present study. Also the middle peak at 8.9 eV is more clearly separated and the highest third maximum is at 9.6 eV. The present coincidence study of the electronic structure of the Se_6 cluster shows that it can be characterized by double peak shape with maxima at 8.6 eV and 9.1 eV, but in Ref. 10 one single asymmetric broadband structure was reported, in binding energy range between 8 and 10 eV. The yield of Se_7^+ resembles to the abundance distribution of the Se_6 clusters, but the higher peak is shifted to 8.7 eV and the lower is detectable at 8.1 eV.

The variances in the spectra of the Se_{5-7}^+ clusters compared with the earlier coincidence study[10] may be caused by the substantial influence of changes in thermodynamic conditions to the formation of isomeric distribution of microclusters. A possible explanation for the discrepancies with Ref. 10 can be found in the isomeric distribution of the clusters in the vapor. As the thermodynamic conditions of the cluster formation vary, they can produce clusters of the same size but with very different abundancies of isomers. As demonstrated by the horizontal bars in Figure 4, different isomers of, e.g., Se_5 and Se_6 have drastically different energy level structures and even relatively small changes in isotopic abundances should be immediately reflected in the valence photoelectron spectra.

IV. DISCUSSION

A. Correlation between the ionization, dissociation energies, and gas phase enthalpies of the formation of the Se clusters.

The fragmentation of different sizes of clusters can be studied by PIY measurements, following ion production as a function of the ionizing photon energy or by PEPICO technique extracting information from CIY curves. The PIY curves in VUV energy range enable an accurate determination of adiabatic ionization energies depending on the cluster size. The adiabatic ionization energy IE(M) of a cluster M is connected to the enthalpy of the formation (or heat of formation) of an ion in the gas phase $\Delta_f H(M^+)$. Its value can be obtained through a simple treatment of the thermochemistry of the ionization process.[23] The corresponding relation may be formulated as

$$\Delta_f H(M^+) = \Delta_f H^o(M) + \mathrm{IE}(M), \tag{2}$$

where $\Delta_f H^o(M)$ is the enthalpy of the formation of a neutral cluster (or molecule). Similarly, the enthalpy of formation of a positive fragment cluster ion, A^+, from precursor cluster AB, is given by

$$\Delta_f H(A^+) = \Delta_f H^o(AB) - \Delta_f H^o(B) + \mathrm{AE}(A^+), \tag{3}$$

where the appearance energy AE(A^+) of fragment is equal to the sum of dissociation energy, $D^+(AB)$, and the ionization energy of the precursor cluster,

$$\mathrm{AE}(A^+) = \mathrm{IE}(AB) + D^+(AB). \tag{4}$$

Here, it is assumed that there is no potential barrier in the reaction coordinate for the processes.

Now let us consider the following ionization and dissociation reactions of selenium clusters Se_n and Se_{n-p}, where $n > p$:

$$\mathrm{Se}_n + h\nu \rightarrow \mathrm{Se}_n^+ + e^-, \tag{5}$$

$$\mathrm{Se}_{n-p} + h\nu \rightarrow \mathrm{Se}_{n-p}^+ + e^-, \tag{6}$$

$$\mathrm{Se}_n^+ \rightarrow \mathrm{Se}_{n-p}^+ + \mathrm{Se}_p, \tag{7}$$

$$\mathrm{Se}_n \rightarrow \mathrm{Se}_{n-p} + \mathrm{Se}_p. \tag{8}$$

Corresponding equations connecting the spectroscopic and thermodynamic characteristics are, respectively,

$$\Delta_f H(\mathrm{Se}_n^+) = \Delta_f H^o(\mathrm{Se}_n) + \mathrm{IE}(\mathrm{Se}_n), \tag{9}$$

$$\Delta_f H(\mathrm{Se}_{n-p}^+) = \Delta_f H^o(\mathrm{Se}_{n-p}) + \mathrm{IE}(\mathrm{Se}_{n-p}), \tag{10}$$

$$\Delta_f H(\mathrm{Se}_{n-p}^+) = \Delta_f H^o(\mathrm{Se}_n^+) - \Delta_f H^o(\mathrm{Se}_p) + D_{n,p}^+, \tag{11}$$

$$\Delta_f H(\mathrm{Se}_{n-p}) = \Delta_f H^o(\mathrm{Se}_n) - \Delta_f H^o(\mathrm{Se}_p) + D_{n,p}. \tag{12}$$

TABLE II. Calculated neutral $D_{n,p}$ and ion $D^+_{n,p}$ dissociation energies of Se_n clusters at $T = 513$K (ion dissociation energies given in brackets). Here the letter p denotes a number of atoms in a neutral fragment. The calculated enthalpies of formation of different clusters (based on the standard enthalpies from Ref. 25) and measured experimental ionization energies are given in the second and third column, respectively. Here the values of IEs are equalized with AEs that are given in Table I.

			$D_{n,p}$ ($D^+_{n,p}$)						
n	${}_fH^o(Se_n)$	IE(Se_n)	$p=1$	$p=2$	$p=3$	$p=4$	$p=5$	$p=6$	$p=7$
1	2.47	9.75							
2	1.43	8.84	3.52						
			(4.43)						
3	1.97	9.58	1.94	1.94					
			(1.20)	(2.11)					
4	1.87	9.14	2.58	1.00	2.58				
			(3.02)	(0.70)	(3.19)				
5	1.73	7.93	2.61	1.67	1.67	2.61			
			(3.82)	(3.32)	(2.58)	(4.43)			
6	1.70	8.24	2.51	1.60	2.24	1.60	2.51		
			(2.19)	(2.50)	(3.58)	(2.20)	(4.02)		
7	1.90	7.94	2.27	1.26	1.94	1.94	1.26	2.27	
			(2.57)	(1.25)	(3.13)	(3.57)	(2.16)	(4.08)	
8	2.02	8.11	2.35	1.11	1.68	1.71	1.68	1.11	2.35
			(2.19)	(1.24)	(1.50)	(2.75)	(3.15)	(1.84)	(4.00)

Now, combining Eqs. (9)–(12), one leads to the relation

$$D^+_{n,p} = D_{n,p} + \mathrm{IE}(Se_{n-p}) - \mathrm{IE}(Se_n), \quad (13)$$

what gives the dissociation energy of a Se_n^+ cluster connected to the fragmentation energy of the corresponding neutral Se_n cluster plus the difference of ionization energies of the fragment and precursor cluster. The neutral dissociation energy $D_{n,p}$, corresponding to the reaction (8), may be estimated by combining enthalpies of the formation of neutral precursor and fragment clusters.[24] In order to evaluate an increase in the enthalpy with temperature, the corresponding dependence of the heat capacities of the clusters need to be taken into account.[25]

However, before going further it should be noted that the preferential fragmentation pathways are, instead of the enthalpy change of the system, governed by the free energy change which takes into account the possible existence of different isomers of the fragments at finite temperature. An increasing role of the entropy contribution to the free energy of clusters, as the most rapidly rising function of the cluster size has been shown in Ref. 26. For comparison, the investigation of thermal effects on the equilibrium geometric structure and size distribution of Si_4, Si_5, Si_6 clusters neither find any thermally induced stabilization of metastable cluster geometries, nor any large changes in the entropy with changing cluster which would change the abundances.[27] According to *ab inito* molecular dynamics studies of the selected microclusters of Na, Si, and Mg at finite temperatures the residence time in one specific isomer as well its temperature range of "rigidity" depend strongly on the size of the cluster. Additionally, the changes in the vibrational spectra are far more influenced by the structural than electronic properties (especially for Na clusters).[28] From the study of the photothermodissociation of Se clusters has been obtained that the entropy contribution affects the dissociation energy values less than ± 0.1 eV, but it is essential to consider the entropy to ensure the consistency within the dissociation rates.[12] Taking into account the above-mentioned circumstances, the interpretation of CIYs of Se clusters are constrained only in view of the enthalpy change in the present study. The calculated dissociation energies for Se_{1-8} clusters are presented in Table II. In these calculations it is assumed that the onsets of PIY curves do not contain ion signals from fragmentation products and the values of ionization energies are equalized with appearance energies that are given in Table I.

These calculated dissociation energies can now be used to predict the preferential dissociation pathways of VUV-ionized Se_n clusters. The analysis of Table II indicates that for ions Se_3^+, Se_4^+, and Se_5^+ the lowest dissociation energy value belongs to the fragmentation channel that produces Se_2^+ dimers. For Se_6^+ cation, there are two energetically almost equal dissociation paths: $Se_2^+ + Se_4$ and $Se_5^+ + Se_1$. However, for larger cluster ions Se_7^+ and Se_8^+, the lowest energy dissociation pathway is again the one that produces Se_2 neutral dimers. For Se_7^+, the channel $Se_7^+ \rightarrow Se_5^+ + Se_2$ requires about 0.9 eV less energy than the next pathway, $Se_7^+ \rightarrow Se_2^+ + Se_5$. These trends in fragmentation channels may be directly related to the fact that the charge is preferably located at the fragment, which has lower ionization energy. However, the most stable clusters are Se_2 and Se_2^+. The last result is confirmed also by the earlier experimental study of Se cluster cations produced by the combination of laser vaporization and supersonic expansion techniques.[13] The very low dissociation energy values for the creation of Se_2^+ fragments from ionized clusters Se_3^+ and Se_4^+ are an indication of high structural instability of Se trimers and tetramers, compared with other Se clusters created in direct evaporation process. The very low intensity of the CIY curves of Se trimers and tetramers below 10 eV, in binding energy scale, is thus in very good agreement with our predictions based on the thermochemical treatment.

B. *Ab initio* calculations of molecular orbitals and fragmentation pathways of Se_n microclusters

The different conformations of Se_n clusters formed in the direct evaporation process cannot be resolved by the used technique, but quantum chemistry modeling offers a glimpse into the geometries of Se_n clusters. More essentially, the electronic properties of modeled clusters provide useful information for interpreting the experimental data. The *ab initio* calculations in this work were performed under the framework of restricted open-shell Hartree-Fock[29] (ROHF) and unrestricted Hartree-Fock with second-order Møeller-Plesset[30] (UMP2) theory with the help of GAMESS (Ref. 31) (The General Atomic and Molecular Electronic Structure System) software. The spin contamination in UMP2 calculations is less than 3% and zero-point energies were taken into account in calculating theoretical appearance energies. Theoretical appearance energies were estimated by subtracting the lowest total energy of the neutral parent cluster from the sum of total energies of its isolated fragment clusters.

In order to find an extensive conformation number of the $Se_{n=2-7}$ clusters, great numbers of grid points on $3n - 6$ ($n > 2$) dimensional potential surfaces (as functions of internuclear positions) of the Se_n clusters were set as initial geometries for optimization. A compact code written in C++ programming language was used for generating grid points, where angle parameters in z-matrices of the initial geometries were set to vary with 30° steps. The located conformations at a light basis set were re-optimized with higher basis sets 6-31 and 6-31(df) using the ROHF and UMP2 theories, respectively. Molecular orbital energies of the geometry optimized Se clusters were used to qualitatively determine their binding energies (BEs). The MO energies of different conformations of $Se_{n=2-6}$ clusters are presented together with the selenium CIY spectra in Figure 4. The horizontal bars in Figure 4 cover the calculated MO energy ranges of various conformations, starting upwards with the lowest total energy isomers. Every vertical tick marks a MO energy of the isomer.

Se_2: Consider first the Se_2^+ CIY spectrum in Figure 4. The bottom left of Figure 4 displays the Se_2^+ CIY spectrum combined with theoretical BEs calculated using the 6-31/ROHF theory (grey bars) and the 6-31(df)/UMP2 theory (black bars). The calculated BEs agree well with the Se_2^+ CIY spectrum, and a comparison between the BEs of the different methods shows no essential differences in the qualitative features. The valence/outer shell MO energy distributions provided by the different methods are slightly varied, but they both match well with the peaks of Se_2^+ CIY spectrum. In fact, (see the other spectra in Figure 4) further contrasting the MO energies of heavier Se clusters calculated by using the two different methods demonstrates the concord of the results of both methods with the CIY spectra. Thus, the results provided by the ROHF theory at the 6-31 basis level are adequate for interpreting the photoelectron spectra with the given energy resolution of the measurements. Besides, due to the technical limitation of used computational resources all conformations of the selenium clusters, which are found by using the ROHF theory at 6-31 basis set, cannot be searched by using the more accurate method. The following discussion will focus on the calculation results provided by the ROHF method.

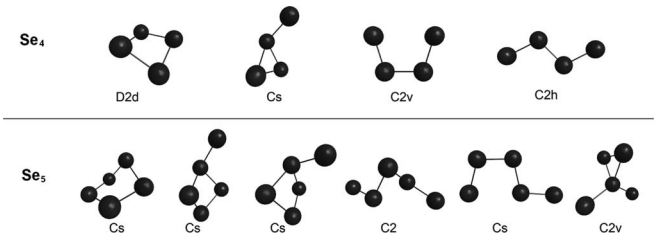

FIG. 5. The different conformations of Se_4 and Se_5 clusters modelled by using the restricted open-shell Hartree-Fock theory with the split-valence 6-31 basis set with the help of GAMESS and MACMOLPLT softwares. The total energy of cluster isomers increases from left to right. The labels mark a symmetry of isomers.

Se_3: In the right bottom panel of Figure 4 calculation results for two conformers of Se_3 are given. The lower one of the ROHF results is for an equilateral triangle (D_{3h}) and the upper one (with 0.7 eV higher total energy) corresponds to the open triangle geometry (C_{2v}). The total energy order of the two conformations is opposite under the framework of 6-31(df)/UMP2, but the total energy difference is only 0.01 eV. As mentioned in Sec. IV A, Se_3 and Se_4 clusters are hardly at all formed, at least in the production by direct vacuum evaporation conditions. Taking into account the energy positions of the highest occupied molecular orbitals (HOMO) for both Se_3 isomers that are clearly and quite far below the onset of strong TOF signal above 10.2 eV, it may be concluded that neutral Se_3 still exists in initial cluster's beam. However, in a spectrum of Se_3^+ one can see great intensities above 10.2 eV. This high CIY signal may be interpreted (see also Table II) as a result of ejected photoelectrons from dissociating bigger clusters, such as Se_5, Se_6, and Se_7 clusters. In other words, the spectrum shows photoelectrons in coincidence with Se_3^+ cationic fragments, not with parent Se_3^+ clusters.

Se_4: A similar feature, the late gain of CIY intensity, can also be seen in the spectrum of Se_4 ions. In the case of Se tetramer four different isomer's geometries have been calculated (see Figure 5). These four isomers from left to right in the upper panel of Figure 5 and in increasing sequence of total energy have D_{2d}, C_s, C_{2v}, C_{2h} symmetries separated by 0.95 eV, 0.24 eV, and 0.27 eV, respectively.

Se_{5-7}: In the right middle panel of Figure 4 the MOs for six distinct conformation of Se_5 clusters are depicted. According to the calculations, the first peak at the binding energy of 8.0 eV in the spectrum corresponds solely to the HOMO energy of Se_5 cluster with geometry symmetry C_s (see also the lower panel of Figure 5). Intensities in the region with greater binding energy are mostly the sum of intensities of the photoelectrons departed from various MOs of different Se_5 conformations (see Figure 5). These six isomers from bottom to top in increasing sequence of total energy have separated by 1.71 eV, 0.03 eV, 0.92 eV, 0.08 eV, and 0.54 eV, respectively.

A peak and its shoulder in CIY spectrum in left top panel of Figure 4 sit well on the calculated BEs of valence MOs of Se_6 clusters. It is noteworthy that photoelectron intensities drop to the background signal level at the binding energy of 10.0 eV. However, the calculations of MO levels for nine different conformation of Se_6 show high number of orbitals above 10 eV. In other words, very low signal of

TABLE III. Photodissociation pathways for Se_n clusters of different size ($n = 3$–7) given together with corresponding *ab initio* calculated appearance energies using the ROHF and UMP2 theories, AE_1 and AE_2. The last column contains values of appearance energy, AE_3, that are derived using Eqs. (4) and (13).

Fragments	Parent cluster	AE_1 (eV)	AE_2 (eV)	AE_3 (eV)
Se, Se_2^+	Se_3	10.77	11.91	10.8
Se^+, Se_2	Se_3	11.73	13.99	11.7
Se^+, Se, Se	Se_3	14.73	19.84	...
Se_2^+, Se_2	Se_4	9.87	9.42	9.8
Se, Se_3^+	Se_4	10.64	11.73	12.2
Se^+, Se_3	Se_4	11.38	13.17	12.3
Se, Se, Se_2^+	Se_4	12.88	15.27	...
Se^+, Se, Se_2	Se_4	13.83	17.35	...
Se_2^+, Se_3	Se_5	10.32	9.86	10.5
Se_2, Se_3^+	Se_5	10.54	10.50	11.2
Se, Se_4^+	Se_5	11.15	11.94	11.8
Se^+, Se_4	Se_5	12.18	14.43	12.4
Se, Se, Se_3^+	Se_5	13.55	16.35	...
Se^+, Se, Se_3	Se_5	14.28	17.79	...
Se, Se, Se, Se_2^+	Se_5	15.78	19.9	...
Se^+, Se, Se, Se_2	Se_5	16.74	21.97	...
Se_3^+, Se_3	Se_6	10.66	...	11.8
Se_2, Se_4^+	Se_6	10.72	...	10.7
Se, Se_5^+	Se_6	10.77	...	10.4
Se_2^+, Se_4	Se_6	10.79	...	10.4
Se^+, Se_5	Se_6	11.85	...	12.3
Se_2^+, Se_2, Se_2	Se_6	12.35	...	...
Se, Se_2^+, Se_3	Se_6	12.90	...	...
Se, Se_2, Se_3^+	Se_6	13.12	...	...
Se, Se, Se_4^+	Se_6	13.73	...	...
Se^+, Se_2, Se_3	Se_6	13.85	...	...
Se^+, Se, Se_4	Se_6	14.75	...	...
Se, Se, Se, Se_3^+	Se_6	16.12	...	...
Se^+, Se, Se_2, Se_2	Se_6	16.31	...	...
Se^+, Se, Se, Se_3	Se_6	16.86	...	...
Se_5^+, Se_2	Se_7	9.93	...	9.2
Se_2^+, Se_5	Se_7	10.05	...	10.1
Se_4^+, Se_3	Se_7	10.43	...	11.1
Se_3^+, Se_4	Se_7	10.72	...	11.5
Se_6^+, Se	Se_7	10.72	...	10.5
Se^+, Se_6	Se_7	11.43	...	12.0

photoelectrons, detected in coincidence with Se_6 cluster cations above binding energy equal to 10 eV, suggests that the Se_6 clusters would dissociate before the detection of the coincidence signal of Se_6^+ ions in this binding energy range. If we look at the spectrum of Se_7 clusters in the right top panel of Figure 4, a similar feature as in the context of Se_6 clusters can be observed – rather weak photoelectron intensities are seen after binding energy higher than 9.5 eV. The same conclusion can be drawn as in the case of Se_6 clusters.

In Table III photofragmentation pathways for clusters $Se_{3–7}$ together with *ab initio* calculated appearance energy values (AE_1 and AE_2) are given. The last column of Table III contains also, for comparison, the values of appearance energies (AE_3), what are derived from Eqs. (4) and (13). The calculated AE_1 values correspond to the conformations with the lowest total energy, respectively. In the case of clusters Se_3, Se_4, and Se_5 the values of AE_1 and AE_3 match very well. For Se_6 and Se_7, a comparison of the values of AE_1 and AE_3 shows already some discrepancies in energy sequence. These differences can be explained by the increased number of possible isomers participating in different dissociation channels. Hence, the appearance energy of one definite dissociation pathway is not determined by the isomer with the lowest total ground state energy, but is affected by distribution of different conformations at fixed temperature.

Now, using the values of AE_3 for the clusters Se_6 and Se_7 in Table III and the dissociation energies of Se_8 in Table II, it is possible to give more detailed interpretation of CIYs in Figure 4. The peaks of clusters Se_6^+ and Se_7^+ below the 10 eV of binding energy are caused by ionization of the corresponding neutral clusters. The high energy shoulder of cluster Se_6 may also contain weak fragment signal from dissociation of a cluster Se_8, but above the binding energy equal to 9.3 eV. In the case of the CIY of cluster Se_5^+, the maximum at 9.5 eV is clearly above the appearance energy of a fragment pair Se_2, Se_5^+ created in dissociation of cluster Se_7. The strong maximum of CIY of Se_4^+ cluster at 11.1 eV has substantial contribution from fragmentation process $Se_6 + h\nu \rightarrow Se_4^+ + Se_2$ and its energetic location coincides with the AE of Se_4^+ and Se_3 from dissociating cluster Se_7. The intensity of the weaker peak at 12.3 eV can be related to the opening of the dissociation pathway $Se_5 + h\nu \rightarrow Se_4^+ + Se$ at binding energy equal to 11.8 eV. The first maximum of the CIY of Se trimer at 11.4 eV may be related to the dissociation of the clusters Se_5, Se_8, and Se_7. The weak maximum at binding energy 12.1 eV is 0.3 eV above the AE of fragmentation pair (Se_3, Se_3^+) from the cluster Se_6. The closest AE to the second higher maximum at 12.8 eV has the decay channel $Se_4 + h\nu \rightarrow Se_3^+ + Se$ at binding energy 12.2 eV. The first peak at 9.0 eV of the spectrum of the Se dimer can be interpreted as an ionization of HOMO of initially neutral Se dimer. The next maximum at 10.7 eV is already above the AE level of all bigger Se clusters in this experiment. The third most intense structure in binding energy range from 12 eV to 14 eV contains electron signal, what is caused by the ionization of higher orbitals of Se_2 fragments from different larger Se clusters and multiple dissociation processes.

V. CONCLUSIONS

In this study the valence electronic structure of the Se_n clusters ($n \leq 8$), produced by direct vacuum evaporation, has been investigated by using the PEPICO technique together with the PIY detection. The ionization and appearance energies of the clusters have been calculated and compared with the experimental results. The dissociation energies of Se_n clusters were derived from the recurrent relation between the gas phase enthalpies of the formation of corresponding cationic clusters and experimental ionization energies.

It was shown that PEPICO technique combined with *ab initio* calculations of dissociation (and appearance) energies is a very useful experimental tool for the size-selective exploration of the electronic structure of microclusters and their fragmentation dynamics. The consistent interpretation for CIYs of all detected Se clusters based on calculated

appearance and dissociation energies was given. The coincidence signals from eight selenium clusters (from Se_1 up to Se_8) were detected. The existence of (unstable) neutral Se trimers and tetramers in a direct vacuum evaporation has been detected. The high intensity structures in the CIYs of clusters Se_3^+ and Se_4^+ are caused by the different fragmentation channels of larger Se clusters. According to the analysis of the derived dissociation energies of Se_n^+ clusters, the lowest fragmentation energy have decay channels that lead to the creation of singly charged Se dimers from clusters Se_{3-6}^+ and neutral Se dimers from bigger clusters Se_7^+, Se_8^+. The comparison of the experimental and theoretical ionization energies and CIY curve for one definite cluster indicates that the experimental adiabatic ionization energy is not always determined by the isomer, which has the lowest total energy. The adiabatic ionization energy is determined, on the contrary, by the number of possible isomers and by their abundance at fixed temperature.

ACKNOWLEDGMENTS

The experimental and theoretical work of this project was supported by the Academy of Finland, the Turku University Foundation, Nordforsk Infrastructure Network "Advanced spectroscopy using MAX-laboratory in Lund" and the EU "Transnational Access to Research Infrastructures" programme. The members of the electron spectroscopy group of the University of Oulu are acknowledged for their role in developing the PEPICO setup and sharing the equipment. Also the help of the staff of MAX-lab is greatly appreciated.

[1]N. Ralston, Nat. Nanotechnol. **3**, 527 (2008).
[2]P. Tran *et al.*, Int. J. Nanomedicine **3**, 391 (2008).
[3]K.-S. Liao, Chem. Phys. Lett. **484**, 242 (2010).
[4]J. Berkowitz *et al.*, J. Chem. Phys. **48**, 4346 (1968).
[5]J. Becker *et al.*, Z. Phys. D **19**, 233 (1991).
[6]D. Hohl, R. O. Jones, R. Car, and M. Parrinello, Chem. Phys. Lett. B **139**, 540 (1987).
[7]Z. Q. Li, J. Z. Yu, K. Ohno, B. L. Gu, R. Czajka, A. Kasuya, Y. Nishina, and Y. Kawazoe, Phys. Rev. B **52**, 1524 (1995).
[8]S. Kohara, A. Goldbach, N. Koura, M.-L. Saboungi, and L. A. Curtiss, Chem. Phys. Lett. B **287**, 282 (1998).
[9]B. C. Pan, J. G. Han, J. Yang, and S. Yang, Phys. Rev. B **62**, 17026 (2000).
[10]J. Becker, K. Rademann, and F. Hensel, Z. Phys. D **19**, 229 (1991).
[11]B. Tribollet, A. Benamar, D. Rayane, P. Melinon, and M. Broyer, Z. Phys. D **26**, 352 (1993).
[12]C. Bréchignac, P. Cahuzac, N. Kébaïli, and J. Leygnier, J. Chem. Phys. **112**, 10197 (2000).
[13]X. Yang, Y. Hu, S. Yang, and M. M. T. Loy, J. Chem. Phys. **111**, 7837 (1999).
[14]*Frontiers of Coincidence Experiments*, in J. Electron. Spectrosc. Relat. Phenom., edited by K. Ueda (Elsevier, 2004), Vol. 141.
[15]O. Kostko, S. R. Leone, M. A. Duncan, and M. Ahmed, J. Phys. Chem. A **114**, 3176 (2010).
[16]K. Rademann, Ber. Bunsenges. Phys. Chem. **93**, 653 (1989).
[17]M. Patanen, S. Urpelainen, M. Huttula, R. Sankari, V. Kisand, E. Nõmmiste, E. Kukk, H. Aksela, and S. Aksela, Phys.Rev. A **80**, 013414 (2009).
[18]S. Urpelainen, M. Huttula, T. Balasubramanian, R. Sankari, P. Kovala, E. Kukk, E. Nõmmiste, S. Aksela, R. Nyholm, and H. Aksela, AIP Conf. Proc. **1234**, 411 (2009).
[19]E. Kukk, R. Sankari, M. Huttula, A. Sankari, H. Aksela, and S. Aksela, J. Electron. Spectrosc. Relat. Phenom. **155**, 141 (2007).
[20]M. Huttula, S. Heinäsmäki, H. Aksela, E. Kukk, and S. Aksela, J. Electron. Spectrosc. Relat. Phenom. **156–158**, 270 (2007).
[21]R. S. Freund, R. C. Wetzel, R. J. Shul, and T. R. Hayes, Phys. Rev. A **41**, 3575 (1990).
[22]D. G. Streets and J. Berkowitz, J. Electron. Spectrosc. Relat. Phenom. **9**, 269 (1976).
[23]S. G. Lias and J. E. Bartmess, "Gas-phase ion thermochemistry," see http://webbook.nist.gov/chemistry/ion/.
[24]P. W. Atkins and J. C. de Paula, *Atkins' Physical Chemistry* (Oxford University Press, New York, 2006).
[25]Å. Olin, B. Noläng, L.-O. Öhman, E. G. Osadchii, and E. Rosén, *Chemical Thermodynamics Series Volume 7: Chemical Thermodynamics of Selenium* (Elsevier Science, Amsterdam, 2005).
[26]C. Bréchignac, Ph. Cahuzac, M. de Frutos, N. Kébaïli, and A. Sarfati, Phys. Rev. Lett. **77**, 251 (1996).
[27]D. Tománek, C. Sun, N. Sharma, and L. Wang, Phys. Rev. B **39**, 5361 (1989).
[28]U. Röthlisberger and W. Andreoni, Z. Phys. D **20**, 243 (1991).
[29]F. W. Bobrowicz and W. A. Goddard, in *Modern Theoretical Chemistry*, 3rd ed., edited by H. F. Schaefer (Plenum, New York, 1977), Vol. 3, Chap. 4.
[30]C. M. Aikens, S. P. Webb, R. L. Bell, G. D. Fletcher, M. W. Schmidt, and M. S. Gordon, Theor. Chem. Acc. **110**, 233–253 (2003).
[31]M. W. Schmidt, K. K. Baldridge, J. A. Boatz, S. T. Elbert, M. S. Gordon, J. J. Jensen, S. Koseki, N. Matsunaga, K. A. Nguyen, S. Su, T. L. Windus, M. Dupuis, and J. A. Montgomery, J. Comput. Chem. **14**, 1347 (1993). gamess (see http://www.msg.chem.iastate.edu/gamess/).